Thermal Conductivity of USb2 and UBi2 Single Crystals

Ryszard Wawryk, Jan Mucha, Halina Misiorek, Zygmunt Henkie

Thermal Conductivity of USb2 and UBi2 Single Crystals

Journal:	*Philosophical Magazine & Philosophical Magazine Letters*
Manuscript ID:	TPHM-09-Jun-0269.R1
Journal Selection:	Philosophical Magazine
Date Submitted by the Author:	26-Aug-2009
Complete List of Authors:	Wawryk, Ryszard; Institute of Low Temperature and Structure Research Polish Academy of Sciences Mucha, Jan; Institute of Low Temperature and Structure Research Polish Academy of Sciences Misiorek, Halina; Institute of Low Temperature and Structure Research Polish Academy of Sciences Henkie, Zygmunt; Institute of Low Temperature and Structure Research Polish Academy of Sciences
Keywords:	anisotropy, thermal transport
Keywords (user supplied):	uranium dipnictides, thermal conductivity, anisotropy

Thermal conductivity of USb_2 and UBi_2 single crystals

R. WAWRYK, J. MUCHA, H. MISIOREK, and Z. HENKIE

Institute of Low Temperature and Structure Research Polish Academy of Sciences, 50-950 Wroclaw, P.O. Box 1410, Poland

R.Wawryk@int.pan.wroc.pl

(Received 21 June 2009; final version received)

ABSTRACT

The thermal conductivity (κ) of single crystals of tetragonal uniaxial antiferromagnets USb_2 (T_N = 202 K) and UBi_2 (T_N = 180.8 K) has been measured along the *a*-axis (κ_a) over the temperature range from 0.5 K to 300 K and along the *c*-axis (κ_c) from 0.5 K to 70 K. The as-grown samples have RRR values of about 500 – 600 and 100 – 150 for UBi_2 and USb_2, respectively.

The anisotropy of the thermal conductivity ($\kappa_a(T)/\kappa_c(T)$ ~ 5) and the low-*T* Lorenz ratios are discuss in relation to Fermi surface topology for both compounds.

Keywords: uranium dipnictides, thermal conductivity, anisotropy

§ 1. INTRODUCTION

Uranium compounds display a wide variety of properties that are related to the behaviour of 5*f* electrons. These phenomena vary from one uranium compound to another depending on a number of different factors including crystal structure, crystal electric field (CEF) effects, electronic configuration, etc. Thus, in order to gain a better understanding of the intrinsic nature of 5*f* electron systems, it is useful to examine the evolution of physical properties in series of compounds. For this reason, the series of uranium dipnictides UX_2 (X=P, As, Sb, or Bi) has received considerable attention. These materials become antiferromagnets below room temperature and have ordered magnetic moments and effective paramagnetic moments as large as about 2 μ_B and 3.1 μ_B [1, 2, 3], respectively. Earlier measurements of the magnetic properties of UX_2 compounds were interpreted in terms of localised 5*f* moments of U^{4+} cations in the crystal electric field of the surrounding pnictogen anions [4]. More recent data addressing hyperfine interactions in the UX_2 series, studied by Mössbauer spectroscopy [5], were interpreted in terms of hybridisation between the 5*f* and conduction electrons. The later approach was consistent with the results from angle-resolved photoemission spectroscopy for USb_2 [6], which revealed a narrow, 5*f*-derived band with small dispersion at the Fermi energy. The topology of the Fermi surface of the UX_2 series, when determined either experimentally by de Haas-van Alphen (dHvA) and Shubnikov-de Haas (SdH) measurements [7, 8] or by means of *ab initio* calculations [9], both predict a significant two-dimensional character for the electronic properties. The two dimensional behaviour is thought to vary through the entire series and to reach the clearest difference between USb_2 and UBi_2.

The uranium diantimonide and dibismuthide compounds crystallize in the tetragonal structure of anti-Cu_2Sb type (space group P4/nmm or $\mathbf{D_{4h}^7}$) with two formula units (f.u.) per unit cell. Their lattice parameter ratios *c*/*a* are equal to 2.044 and 2.004, and the Curie-Weiss law determined magnetic moments, μ_{eff}, are equal to 3.32 μ_B and 3.36 μ_B [1, 2, 3, 10, 11], respectively. Neutron diffraction experiments [1]

reveal antiferromagnetic ordering of the uranium magnetic moments, with values of 1.88 μ_B for USb_2 and 2.1 μ_B for UBi_2 below the Néel temperatures, T_N of 202 K and 180.8 K, respectively. The moments are parallel to the *c*-axis and create ferromagnetic planes which alternate perpendicular to the *c*-axis with the sequence (↑↓↓↑) in USb_2 and (↑↓) in UBi_2. This indicates a higher flattening of magnetic Brillouin zone (MBZ) in USb_2 [8] as compared to that in UBi_2. Thus the ratios k_c/k_a, where k_c is the wave vector of the MBZ along the *c*-axis and k_a is the wave vector along the *a*-axis, for USb_2 and UBi_2 are equal to 0.24 and 0.5, respectively.

The Fermi surfaces (FS) and paramagnetic Brillouin zone (PBZ) are basically the same in USb_2 and UBi_2. Roughly speaking the FS consists of two types of branches. The first type of FS branch is a spherical surface and the second is a slightly corrugated cylinder parallel to the *c*-axis [8]. Magnetic ordering in UBi_2 does not change the BZ and hence the FS. The magnetic ordering in USb_2 reduces twice the MBZ and the spherical FS crosses the MBZ and transforms to the two cylinders. The same happens with the corrugated cylinder, which also transforms to the two cylinders. Thus the flattening of the MBZ in USb_2 enhances the two-dimensionality. Consequently, its resistivity anisotropy, which is several times lower than that of UBi_2 at room temperature, becomes several times higher at low-*T* [11]. Here we extend the transport examination to studies of the heat conductivity in USb_2 and UBi_2 single crystals.

§ 2. Experimental Details

The „molten metal solution" method was used to synthesize plate-like single crystals of USb_2 and UBi_2 [12]. From the as-grown crystals, it was possible to prepare rectangular specimens with typical dimensions of about 6.5×1.1×1.3 mm^3 (UBi_2) and 4.0×1.6×0.7 mm^3 (USb_2) along the *a*×*b*×*c* axes for measurements of the thermal conductivity along the *a*-axis, $\kappa_a(T)$, and specimens of about 0.7×0.7×0.6 mm^3 (UBi_2) and 0.6×0.4×1.1 mm^3 (USb_2) along the *a*×*b*×*c* axes for measurements of the thermal conductivity along the *c*-axis, $\kappa_c(T)$. The thermal conductivity was determined with total uncertainty less then 2.5 % by the stationary heat flux method in the temperature range 5 – 300 K and setting the temperature gradient along the specimen's length from the range 0.1 – 0.5 K. The experimental setup and the measurement procedure have been described in detail in ref. [13, 14]. In the range 0.5 K - 80 K the $\kappa(T)$ was measured by the modified set-up for the thermoelectric power measurements [15].

§ 3. Results of the Thermal Conductivity of USb_2 and UBi_2

The *a*-axis thermal conductivity data for USb_2 (specimen $2S^a$) and UBi_2 (specimen $2B^a$) measured in the temperature range 5 K < *T* < 300 K are presented in Fig. 1. The values of κ_a (16.7 and 17.8 W m^{-1} K^{-1} at 300 K for USb_2 and UBi_2, respectively) decrease with temperature down to T_N where $\kappa_a(T)$ traces a shallow valley. Visible change of slope of the $d\kappa_a/dT$ vs. *T* dependence at T_N, as shown in the inset for both compounds, relates this behaviour to the antiferromagnetic ordering temperature. The straight lines following the experimental data and constrained to cross at T_N are used to highlight the anomaly. Though the $\kappa_a(T)$ anomalies at T_N are detectable, they are drastically weaker than the anomalies seen in the electrical resistivities along the *a*-axes shown by two lower curves in the inset, which are due to conduction electron scattering by phonons and fluctuations of magnetic moments [11].

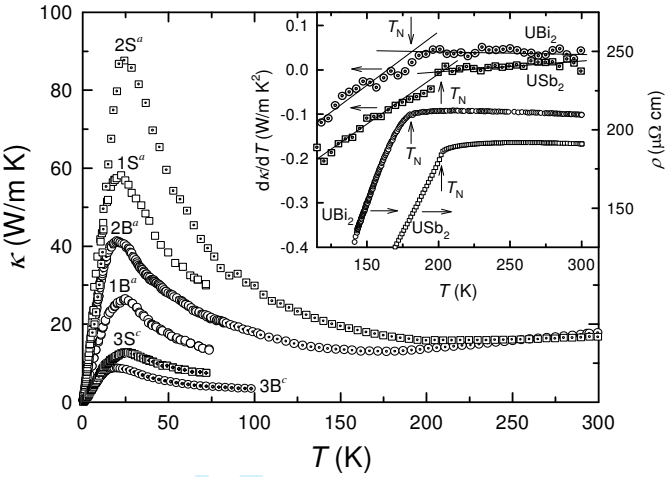

Figure 1. Thermal conductivity of UBi_2 (specimens $1B^a$ and $2B^a$), and USb_2 (specimens $1S^a$ and $2S^a$) single crystals vs. temperature measured along the *a*-axis and $\kappa(T)$ data for UBi_2 (specimen $3B^c$) and USb_2 (specimen $3S^c$) measured along the *c*-axis. The inset presents the derivative $d\kappa_a/dT$ for the specimen's $2B^a$ of UBi_2 and $2S^a$ of USb_2 around the magnetic transition temperature T_N and compares them with the $\rho(T)$ data [11] shown by two lower curves.

For temperature below T_N, $\kappa_a(T)$ passes through a maximum κ_a^{max} at temperature T_{max}, which is dependant on the purity of the specimen, and finally proceeds to zero with decreasing T. In order to better demonstrate the impurity effect, we have determined the low-T behaviour of $\kappa_a(T)$ for several additional specimens prepared from crystals from different batches of USb_2, - specimen (spec.) $1S^a$ – and UBi_2 – spec. $1B^a$. Finally the specimens prepared for measurements of the thermal conductivity along the *c*-axis are denoted $3S^c$ and $3B^c$, respectively. The electrical resistivity, ρ, of each specimen was also examined and residual resistivity ρ_0, for $T \rightarrow 0$, as well as the residual resistivity ratio, RRR = $\rho_{300}/\rho_{4.2}$ were determined; here ρ_{300} and $\rho_{4.2}$ are the resistivities at 300 K and at 4.2 K, respectively. It is well know that higher RRR values often indicate high purity. We can characterize specimens with sets of numbers (RRR):(κ^{max} in W m^{-1} K^{-1}):(T_{max} in K) which are for USb_2 specimens: $1S^a$ - (97):(58):(22); $2S^a$ - (150):(92):(24); $3S^c$ - (2.4):(12.8):(26) and for UBi_2 specimens: $1B^a$ - (498):(26):(24); $2B^a$ - (598):(41):(20); $3B^c$ - (130):(8.7):(18.5).

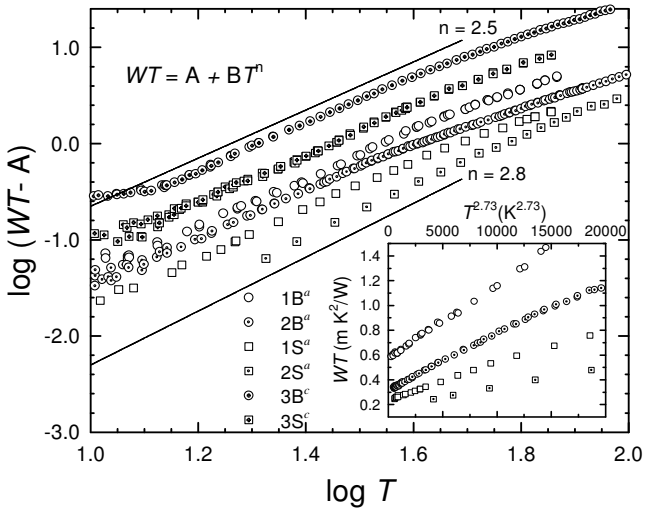

Figure 2. The plot log (WT – A) vs. log T for spec. $1B^a$, $2B^a$, $3B^c$, $1S^a$, $2S^a$, and $3S^c$. The solid lines represent eq. WT = A + BT^n for n = 2.5 and 2.8. The inset shows WT as a function $T^{2.73}$.

We use a metallic approach [16] to analyse the thermal transport in USb_2 and UBi_2 and assume validity of the Wiedemann-Franz-Lorenz law and electronic thermal resistivity $W^e = \rho/LT$ where L is the Lorenz ratio which, under certain conditions, is equal to the standard Lorenz number $L_0 = 2.45 \times 10^{-8}$ W Ω K^{-2}. We assume that for the lowest temperatures $W^e = 1/\kappa^e_{exp}$ is the sum of two components. One is the thermal resistivity due to the scattering of electrons by defects, W^e_d = A/T = ρ_0/L_0T. The

second component is the resistivity due to the scattering of electrons by phonons/magnons $W^e_p = BT^n$ as the examined compounds undergo to antiferromagnetic transitions. Thus,

$$W^e = 1/\kappa^e_{exp} = W^e_d + W^e_p = A/T + BT^n. \quad (1)$$

The power n for scattering by phonons is expected to be 2 at low temperatures and a plot of W^eT against T^3 should give something like a straight line. However, deviation from that expected behaviour is often observed. As a matter of fact, this is the case for USb_2 and UBi_2. The W^eT data for four specimens of these compounds, plotted against $T^{2.73}$ in the inset of Fig. 2, give something like a straight line. More detailed analysis shows that the widest temperature range of linearity is obtained for n selected for particular samples. It is observed that n decreases from 1.8 to 1.5 when W^e increases from the lowest values, as observed for the $2S^a$ specimen, to the highest values for $3B^c$. This is illustrated in main part of Fig. 2 where log (WT - A) data are plotted vs. log T for A values assuring the best linear behaviours in the temperature range of about 10 ─ 50 K. These values of A point out $\kappa_{el} = TL_0/\rho$ approaching or even exceeding κ_{exp} which, however, is expected to be higher then κ_{el}. Such higher values than that expected for A obtained in this approach results presumably from lattice contribution, not negligible in the considered temperature range. This is discussed in the § 4.

Finally we have assumed that the heat transport at the lowest-T (0.5 – 2 K) is entirely controlled by defects. Then $\kappa^e_{exp} = T/A$ comes from eq. (1), allowing us to determine A values as equal to reciprocal of slope of the κ_{exp} vs. T dependence. Such values of A determined at the lowest temperature point to L_0 (in 10^{-8} W Ω K^{-2}) equal to 4.1 and 72 for USb_2 along the a- and c-axis and 0.95 and 10.6 for UBi_2 also along the a- and c-axis, respectively. The values of $\kappa_{el} = TL_0/\rho$ calculated for all these Lorenz numbers are compared in Fig. 3 to corresponding experimental data of the total thermal conductivity in USb_2 and UBi_2 and lattice conductivity, $\kappa_{ph} + \kappa_{mag}$. It is seen that beyond the lowest temperatures the lattice conductivity clearly exceeds the electronic conductivity in the all cases presented in Fig. 3 .

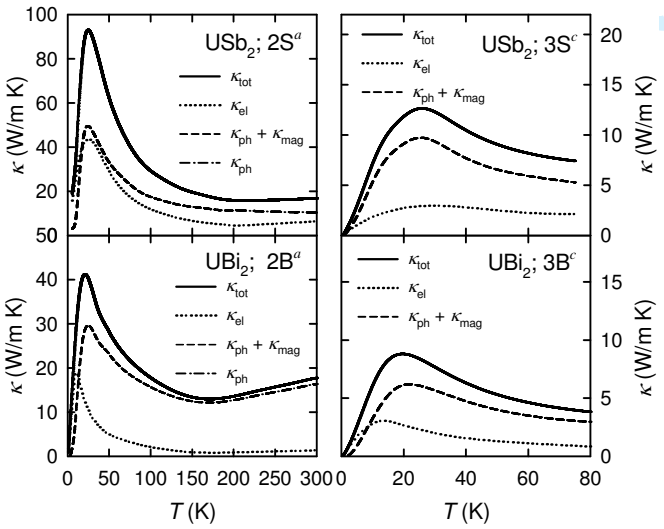

Figure 3. Electronic and phonon/magnon contributions to the total thermal conductivity of USb_2 and UBi_2 single crystals in the a and c directions. The following values of L_0 were taken to evaluation of electronic contribution: 4.1×10^{-8}, 9.5×10^{-9}, 72×10^{-8}, and 10.6×10^{-8} W Ω K^{-2} for the samples $2S^a$, $2B^a$, $3S^c$, and $3B^c$, respectively.

§ 4. Discussion and Summary

Aoki et al. [8] revealed by dHvA and SdH experiments that the spherical α and cylindrical β branches of the FS in UBi_2 occupies 9.9 % and 4.8 % BZ volume, respectively. The magnetic unit cell contains two molecules of UBi_2 and it is expected

to be a compensated metal. Aoki et al. assumed that the spherical α branch is an electron FS and it is compensated with two cylindrical β branches that are the hole Fermi surfaces. This results in either electron and hole carrier concentrations in UBi_2 to be equal 1.1×10^{21} carrier/cm^3 (2×0.099 carrier/$4.44^2\times8.91\times10^{-24}$ cm^3) which is approximately 75 times lower than the concentration of conduction electrons in copper.

The magnetic unit cell of USb_2 contains four molecules of USb_2 and is also expected to be a compensated metal. Its two cylindrical FS, α and δ, originating from spherical FS in the PBZ occupies 16.8 % and 5.4 % of volumes of the magnetic BZ, respectively, and there are two electron FS branches. The two other cylindrical FS type branches, ε and γ, respectively, originating from cylindrical FS branch in PBZ, which occupy 7.9 % and 3.3 % of the MBZ. Aoki et al. assumed that 2ε and 2γ are hole FS branches occupying 22 % of MBZ compensate electron α and δ FS branches thus occupying also 22 % of the MBZ. This results in either electron and hole carrier concentrations in USb_2 to be equal 1.4×10^{21} carrier/cm^3 (2×0.22 carrier/$2\times4.27^2\times8.75\times10^{-24}$ cm^3) which is approximately 61 times lower than the concentration of conduction electrons in copper.

In order to explore a possible correlation between the determined Lorenz number and the topology of the FS, the latter will be characterized, for simplicity, by the difference between its cross section as appropriate for the direction of the thermal conductivity examination and the cross section of spherical surface of a simple metal. For the *a*-axis thermal conductivity of UBi_2, the essential factor will be the shape of the FS cross sections by planes perpendicular k_c. All cylindrical FS branches (2β) are parallel to k_c and their cross sections are circles, like the cross section of the spherical α FS branch. For this case $L_0 = 0.95 \times10^{-8}$ W Ω K^{-2} was found. This value is lower than the standard L_0 value and can be compared with $L_0 = 1\times10^{-8}$ W Ω K^{-2}, as found for ferromagnetic nickel [17].

By comparison to UBi_2, there are 20 % more carriers in USb_2, which form two times as many FS branches. In spite of this difference, the FS are all corrugated cylinders parallel to k_c. Thus the cross sections of the USb_2 FS with planes perpendicular to k_c are composed of six small circles (high curvature) so it is farther from spherical surface of simple metal than in the case of UBi_2. For thermal conductivity along the *a*-axis of USb_2 the value of $L_0 = 4.1\times10^{-8}$ W Ω K^{-2} has been determined. This is in turn higher than the standard L_0 value.

The cylindrical FS branches in UBi_2 can contribute to the transport coefficient along the *c*-axis only as a result of the corrugations in these branches. Any of the cross section with planes parallel to the k_c axis does not resemble cross sections of a spherical surface. The only circular FS cross section may come from the spherical FS α branch, but in spite of this the overall similarity to a spherical cross section is reduced and an increased value of $L_0 = 10.6\times10^{-8}$ W Ω K^{-2} was determined for the *c*-axis thermal conductivity in UBi_2. Finally, L_0 increases up to 72×10^{-8} W Ω K^{-2} in the case of USb_2 for the *c*-axis where all FS branches are corrugated cylinders parallel to k_c.

Based on a simple theoretical treatment, (see ref. [16]) the lattice thermal conductivity should be about one-third of the electronic component at high temperature if only phonon-electron scattering is important. Calculations done for copper show that the lattice contribution gives a very small fraction to the total thermal conductivity at high and low temperatures. It will suffice to remark that at high temperature the ratio $\kappa/\sigma T$ is close to the standard value L_0. This is obviously

not the case of our compounds, which show layered chemical structure and are low carrier density systems. Instead, we make a comparison to the thermal conductivity of $YBa_2Cu_3O_{7-y}$ as examined by Hagen et al. [18]. This material is a low carrier density system with a layered chemical structure and similar thermal conductivity anisotropy in the normal state where $\kappa_{ab}/\kappa_c \approx 5 - 6$. For this compound, it was found that the standard L_0 indicates that the electronic contribution is 55 % of the total κ_{ab} and 1 – 2 % of κ_c. Thus, it was argued that detailed analysis of the latter casts serious doubt about the validity of applying the Bloch-Boltzmann theory to the transport behaviour along the *c*-axis. In the case of USb_2 and UBi_2 the low temperature L_0 behaviour points towards lower contribution of the electronic thermal conductivity to the total conductivity as compared to that determined by standard L_0 in the case of the *a*-axis thermal conductivity of UBi_2 – 10 % - and the higher one in the case κ_{el} for the *a*-axis of USb_2 – 36 % - and κ_{el} for the *c*-axis of USb_2 – 38 % - and UBi_2 – 23 %. In the latter case the κ_{el} contribution is nearly 30 times higher than that calculated for standard L_0.

Electronic thermal resistivity due to the scattering of electrons by phonons should show quadratic temperature dependence at low-*T*. In our case, we observe a thermal resistivity term $W \sim T^n$ with *n* decreasing from 1.8 for specimens with the lowest thermal resistivities to 1.5 for specimens with the highest resistivities, on this temperature range (see Fig. 2). The total thermal resistivity seems to be the main parameter controlling the decrease of *n*. Presumably, *n* is an effective parameter, which decreases with an additional scattering mechanism and gives an additional contribution to the total thermal resistivity. At these temperatures, we first consider a lattice term for which the temperature dependant contribution varies like T^{-2} and increases with increasing ρ_0. The lattice thermal conductivity would be about one-third of the electronic component at high temperature if only phonon-electron scattering was important in determining both contributions [16]. As the examined compounds are antiferromagnets, we should also consider the possible scattering of electrons by magnetic moments, for which the contribution to the electronic thermal conductivity seems to be well described by $\kappa_{el}(T) = L_0T/\rho(T)$. Therefore it is surprising that the $\kappa_a(T)$ data for both compounds show weak anomalies at T_N as compared with $\rho_a(T)$ (inset to Fig. 1). There also is a weak and weakly temperature dependent anisotropy of the thermal conductivity. The ratio $\kappa_a(T)/\kappa_c(T)$ at 80 K (maximum of $\rho_c(T)$ for USb_2) for the best specimens of USb_2 and UBi_2 is equal to 5.1 and 5.4, respectively, and does not change by more than 30 % with temperature down to 20 K. This result can be compared with the anisotropy of the electrical resistivity, as shown for the both compounds by the lower inset in Fig. 4.

To show high specimen sensitivity of another electronic transport coefficient, we present thermoelectric power for specimen $2S^a$ showing RRR 150 and compare it with the previously examined specimen $3S^a$ [11]. The increase of RRR enhances the phonon drag peak but lowers the thermoelectric power in the paramagnetic region. One might think that the weak manifestation of the aforementioned peculiarities of electrical resistivity behaviour in the thermal conductivity are possibly due to their signatures being overwhelmed by another scattering mechanism which dominates the total thermal conductivity.

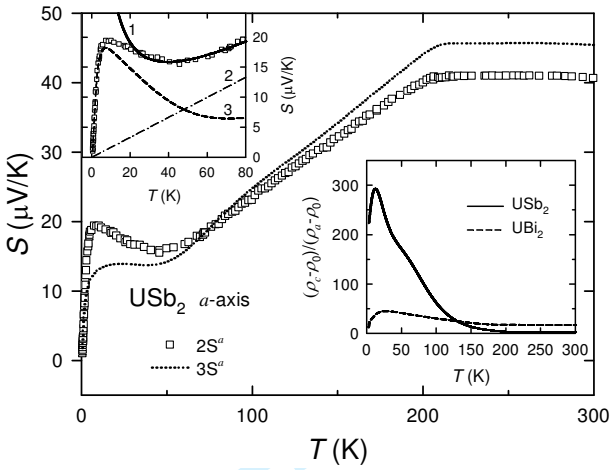

Figure 4. Thermoelectric power vs. temperature for USb_2 single crystals along the *a*-axis. The squares denote the data for $2S^a$ sample, while the dotted line represents the data for $3S^a$ sample measured earlier [11]. Curve 1 in the upper inset displays the equation: $S(T) = aT + b/T$ with the fitting parameters a and b equal to 0.205 μV K^{-2} and 285 μV, respectively. The straight line 2 and curve 3 present the diffusion and phonon/magnon drag contributions to the total thermoelectric power, respectively. The lower inset presents the ratio $(\rho_c - \rho_0)/(\rho_a - \rho_0)$ for USb_2 and UBi_2 single crystals taken from ref. [11].

We conclude that the electronic thermal transport analysis at low temperatures leads to an estimation of various values of the Lorenz number L_0 and gives a more realistic electronic contribution κ_{el} to the total thermal conductivity for both compounds UBi_2 and USb_2. The lack of the spherical FS branches in USb_2 and flat MBZ influence on the anisotropy of the electronic thermal conductivity $\kappa_{el}^a/\kappa_{el}^c$ that is not so large as in electrical resistivity and thermoelectric power. The anisotropy of the total thermal conductivity is comparable with the other layered structures e.g. mentioned above YBCO.

ACKNOWLEDGEMENTS

The authors are indebted to Dr. R.E. Baumbach for his assistance at the manuscript editing.

REFERENCES

[1] J. Leciejewicz, R. Troć, A. Murasik, and A. Zygmunt, *Phys. Stat. Sol.* **22** 517 (1967).
[2] W.Trzebiatowski, A. Sępichowska and A. Zygmunt, *Bull. Acad. Polon. Sci., Ser. Sci. Chim.* **12** 687 (1964).
[3] W. Trzebiatowski and A. Zygmunt, *Bull. Acad. Polon. Sci., Ser. Sci. Chim.* **14** 495 (1966).
[4] G. Amoretti, A.Blaise, and J. Mulak, *J. Magn. Magn. Mater.* **42** 65 (1983)
[5] S. Tsutsui, M. Nakada, S. Nasu, Y. Haga D. Aoki, P. Wiśniewski, and Y. Ōnuki, *Phys. Rev.* B **69** 054404 (2004).
[6] E. Guziewicz, T. Durakiewicz, M.T. Butterfield, C.G. Olson, J.J. Joyce, A.J. Arko, J.L. Sarrao, D.P. Moore, and L. Morales, *Phys. Rev.* B **69** 045102 (2004).
[7] D. Aoki, P. Wiśniewski, K. Miyake, N. Watanabe, Y. Inada, R. Settai, E. Yamamoto, Y. Haga and Y. Ōnuki, *J. Phys. Soc. Jpn.* **68** 2182 (1999).
[8] D. Aoki, P. Wiśniewski, K. Miyake, N. Watanabe, Y. Inada, R. Settai, E. Yamamoto, Y. Haga and Y. Ōnuki, *Philos. Mag.* B **80** 1517 (2000).
[9] S. Lebègue, P.M. Oppeneer, and O. Eriksson, *Phys. Rev.* B **73** 045119 (2006).
[10] R. Troć, L. Shlyk, D. Kaczorowski, M. Potel, H. Noël, A. Pietraszko, in Landolt-Börnstein Numerical Data and Functional Relationships in Science and

Technology, Group III: Condensed Matter , Vol. **27**, Subvol. B **7** (Springer, 2005) p. 229.
[11] R. Wawryk, *Philos. Mag.* **86** No 12 1775 (2006).
[12] Z. Henkie, R. Maślanka, P. Wiśniewski, R. Fabrowski, P.J. Markowski, J.J. Franse and M. van Sprang, *J. Alloys Comp.* **181** 267 (1992).
[13] A. Jeżowski, J. Mucha, G. Pompe, *J. Phys.* D: *Appl. Phys.* **20** 1500 (1987).
[14] J. Mucha, S. Dorbolo, H. Bougrine, K. Durczewski, M. Ausloos, *Cryogenics* **44** 145 (2000).
[15] R. Wawryk and Z. Henkie, *Philos. Mag.* B **81** 223 (2001).
[16] R. Berman: Thermal Conduction in Solids (Oxford: Clerandon Press 1976) p. 147.
[17] G.K. White and R.J. Tainsh, *Phys. Rev.Lett.* **19** 165 (1967).
[18] S.J. Hagen, Z.Z. Wang, and N.P. Ong, *Phys. Rev*. B **40** 9389 (1989).